

# Silicon Sensor Irradiation Studies for the LHC HL Upgrade



BROWN

Andrew Thomas Kent

Department of Physics  
Brown University

Submitted in partial satisfaction of the requirements for the  
Degree of Master of Science  
in Physics

*Advisor:* Professor Ulrich Heintz

May 2022

© 2022 - Andrew Thomas Kent

All rights reserved.

*This thesis by Andrew Thomas Kent is accepted in its present form by the  
Department of Physics as satisfying the thesis requirement for the degree of Master  
of Science.*

.....  
Date                  Ulrich Heintz, Advisor

Recommended to the Graduate Council

.....  
Date                  Andrew G. Campbell, Dean of the Graduate School

*This work is dedicated to my parents, Zaida Soriano and Ron Kent.*

# Acknowledgements

I am very grateful to have had many people help me along the way in my pursuit of an education in physics, and I especially wanted acknowledge a few of those who especially helped me with my goals.

Before arriving at Brown University I received extensive mentoring from Distinguished Professor of Physics at UCLA, George Morales - we would meet every week for a few hours and he would teach me what it meant to be a theoretical physicist and how one should go about solving very difficult problems. I will always look back fondly on those meetings I had with him.

While at UCLA I was the recipient of the Nicholas Dieter Memorial Scholarship which was awarded by former U.S. Ambassador Robert J. Dieter and Mrs. Gwynneth Dieter, their kind words and support helped me quell many doubts I had about the future.

I would like to thank Professor Ulrich Heintz for allowing me to learn in his lab as a laboratory assistant and also for his guidance in writing this thesis, my time working in his lab has been a wonderful education.

Also, from the Brown University Silicon Lab I would like to whole heartedly thank Eric Spencer and Nick Hinton. Eric taught me almost all of the techniques and skills I used in my research presented in this thesis, and I am very grateful for all his support.

Finally, I would like to thanks my family, friends, my girlfriend Yasemin Kirac and most especially my mother. At every step of the way she has supported me. When I decided to switch my path from cooking professionally to going back to school and pursuing physics she was my number one fan, and for that and an incomprehensible list of other supportive things she has done for me, I am eternally grateful.

# Abstract

Hello, this is my abstract

# Table of Contents

<b>Dedication</b>	<b>iii</b>
<b>Acknowledgements</b>	<b>iv</b>
<b>Abstract</b>	<b>v</b>
<b>1 Introduction</b>	<b>1</b>
1.1 The Large Hadron Collider . . . . .	1
1.1.1 The High-Luminosity Large Hadron Collider (HL-LHC) . . . . .	1
1.2 The Compact Muon Solenoid Experiment at CERN . . . . .	3
1.2.1 Silicon Sensors . . . . .	4
1.2.1.1 Pixel Detectors . . . . .	4
1.2.1.2 Strip Sensors . . . . .	4
<b>2 Silicon Detectors</b>	<b>5</b>
2.1 Silicon Sensor Properties . . . . .	5
2.1.1 PN Junction . . . . .	6
<b>3 Radiation Damage</b>	<b>11</b>
3.1 Bulk Silicon Damage . . . . .	11
3.2 Non-Ionizing-Energy-Loss (NEIL) Hypothesis . . . . .	12
3.3 Annealing . . . . .	13
3.3.1 Leakage Current . . . . .	13
3.3.2 Effective Doping Concentration $N_{eff}$ . . . . .	14
3.3.3 Hamburg Annealing Model . . . . .	14
<b>4 Probe Station Experimental Setup</b>	<b>16</b>
4.1 Test Diodes . . . . .	16
4.1.1 DZero Diodes . . . . .	16

4.1.2	PIN Diodes . . . . .	16
4.1.3	2S and PSS Halfmoon Diodes . . . . .	16
4.1.4	HGCAL Diodes . . . . .	16
4.2	Electrical Characterization . . . . .	16
4.2.1	Current-Voltage Measurement (IV) . . . . .	16
4.2.2	Capacitance-Voltage Measurement (CV) . . . . .	16
4.3	Environmental Control . . . . .	16
4.3.1	Temperature Control . . . . .	16
4.3.2	Dew-Point Control . . . . .	16
4.3.3	Humidity Control . . . . .	16
<b>5</b>	<b>Alibava Station Experimental Setup</b>	<b>17</b>
5.1	Test Diodes . . . . .	17
5.1.1	2S and PSS Halfmoon Diodes . . . . .	17
5.2	Radioactive Source . . . . .	17
5.3	Environmental Control . . . . .	17
5.3.1	Temperature Control . . . . .	17
5.3.2	Dew-Point Control . . . . .	17
5.3.3	Humidity Control . . . . .	17
5.4	Measuring Halfmoon Diodes . . . . .	17
5.4.1	Printed Circuit Board . . . . .	17
<b>6</b>	<b>Irradiating at RINSC</b>	<b>18</b>
6.1	Rabbit . . . . .	18
6.1.1	Configuration . . . . .	18
6.1.2	Directionality Studies . . . . .	18
6.1.3	Linear Fluence Intensity Studies . . . . .	18
6.2	Beam-Port . . . . .	18
<b>7</b>	<b>Analysis</b>	<b>19</b>
7.1	Calculating Fluence . . . . .	19
7.1.1	PIN Diodes . . . . .	19
7.1.2	Depletion Voltage Calculation . . . . .	20

7.1.3	Current Temperature Conversion . . . . .	20
7.2	Hamburg Model Analysis . . . . .	20
7.2.1	Ljubljana Diodes . . . . .	20
7.2.2	HGCAL Diodes . . . . .	20
7.3	PIN Analysis . . . . .	20
7.3.1	Temperature Study . . . . .	20
7.3.2	Annealing Study . . . . .	20
<b>8</b>	<b>Conclusions</b>	<b>21</b>
8.1	Use of Diodes in a High Fluence Environment . . . . .	21
8.1.1	PINs . . . . .	21
8.1.2	DZero . . . . .	21
8.1.3	HGCAL . . . . .	21
8.2	Affects of Concurrent Annealing and Irradiation . . . . .	21
8.3	RINSC Ljubljana Cross Calibration . . . . .	21
8.3.1	Silicon Damage Constant . . . . .	21
<b>Bibliography</b>		<b>23</b>
<b>Appendix</b>		<b>24</b>

# List of Figures

1.1	CERN Complex (from [4])	2
1.2	Integrated particle fluence in $1MeV$ neutron equivalent per $cm^2$ for the CMS Phase-2 Tracker (from [17])	3
1.3	CMS Detector Diagram (from [12])	3
2.1	Example of doping in Silicon (from [10])	5
2.2	Pn-junction under electrically neutral conditions (from [2])	6
2.3	Typical IV Curve (from [11])	8
2.4	Typical CV Curve (from [11])	9
3.1	Displacement Damage Functions $D(E)$ (from [9])	13
3.2	Fluence Dependence of Leakage Current for Silicon Detectors (from [9])	14
3.3	Current Related Damage Rate $\alpha$ as a Result of Cumulated Annealing Times at Different Temperatures (from [9])	15
7.1	PIN Fluence Studies at Different Pulsed Currents (from [5])	19

# Chapter 1

## Introduction

### 1.1 The Large Hadron Collider

At the Large Hadron Collider, there are four main experimental setups: CMS, LHCb, Atlas and Alice (as seen in figure 1.1). The Compact Muon Solenoid (CMS) is a multipurpose detector and has been primarily focused on observing new signatures of physics such as the Higgs particle or the lightest supersymmetric particles (SUSY). In order to achieve these objectives, as well as other similar ones, the detector needs to be able to precisely measure the four momenta of the muons, electrons, photons and charged particles over a large energy range [3].

The following chapter will serve as a guide to the LHC in general, with special focus to the coming High-Luminosity LHC upgrade and also to the workings of the CMS detector and it's silicon sensors which serve as the focus of this thesis.

#### 1.1.1 The High-Luminosity Large Hadron Collider (HL-LHC)

The LHC is the world's largest and most powerful particle accelerator [15]. It was built between 1998 and 2008, when it was first started up. The LHC consists of a 27-kilometer ring of super conducting magnets, this ring accelerates the particles to just below the speed of light before they are forced to collide within the designated positions within the detectors. These counter-circulating beams meet with a total collisional energy of 13 TeV at which moment the detectors work to determine the characteristics of the offspring in order to gain insight into the underlying physics which occurred at the moment of collision.

The High-Luminosity LHC (HL-LHC) is a major upgrade of the LHC, the LHC collides tiny particles of matter (protons) in order to study the fundamental com-

## CERN's Accelerator Complex

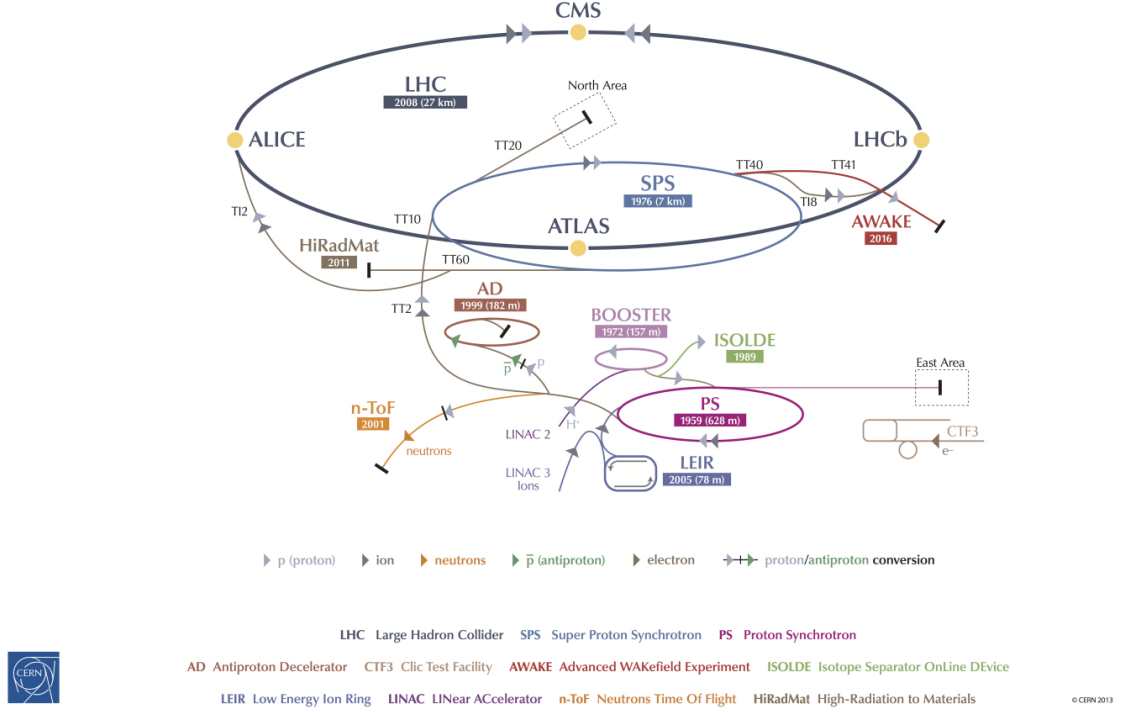


Figure 1.1: CERN Complex (from [4])

ponents of matter and the forces that bind them together, the HL-LHC will allow operators the ability to study these events in more detail by increasing the number of collisions by a factor of 5 – 7 from where they were prior to the upgrade [14]. Luminosity is the measure of the number of potential collisions per surface unit area over a given period of time [14], this quantity integrated is measured in inverse fentobarns [ $fb^{-1}$ ]; where one inverse fentobarn represents 100 million million collisions.

In figure 1.2 we see the integrated particle fluence in 1 MeV neutron equivalent ( $n_{eq}$ ) per  $cm^2$ , where the estimates in the figure correspond to the total integrated luminosity of  $3000 fb^{-1}$  of  $pp$  (proton-proton) collisions at  $\sqrt{s} = 14$  TeV [17]. Of course not all sections of the CMS detector will see the same amount of fluence over the period of operation for phase-2, in figure 1.3 we can see the different layers of CMS where each of the different types of sensors operate. If we compare the two figures, we'll notice that it is expected that the pixel detector could receive up to  $1.0 \cdot 10^{16} MeV n_{eq} cm^{-2}$  while the strip sensors which are housed further from the

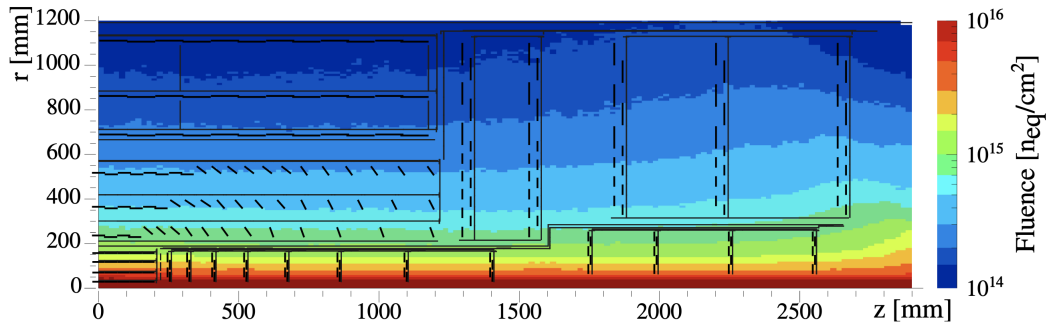


Figure 1.2: Integrated particle fluence in  $1\text{MeV}$  neutron equivalent per  $\text{cm}^2$  for the CMS Phase-2 Tracker (from [17])

beam path could receive up to  $1.0 \cdot 10^{15} \text{ MeV } n_{eq} \text{ cm}^{-2}$  over the course of phase-2 operations. This level of radiation is a concern for any materials, though especially important for the questions of extended accuracy and precision of the silicon particle sensors. It is because of that reasons that there has been extensive research and development of radiation hard materials for the trackers [9].

## 1.2 The Compact Muon Solenoid Experiment at CERN

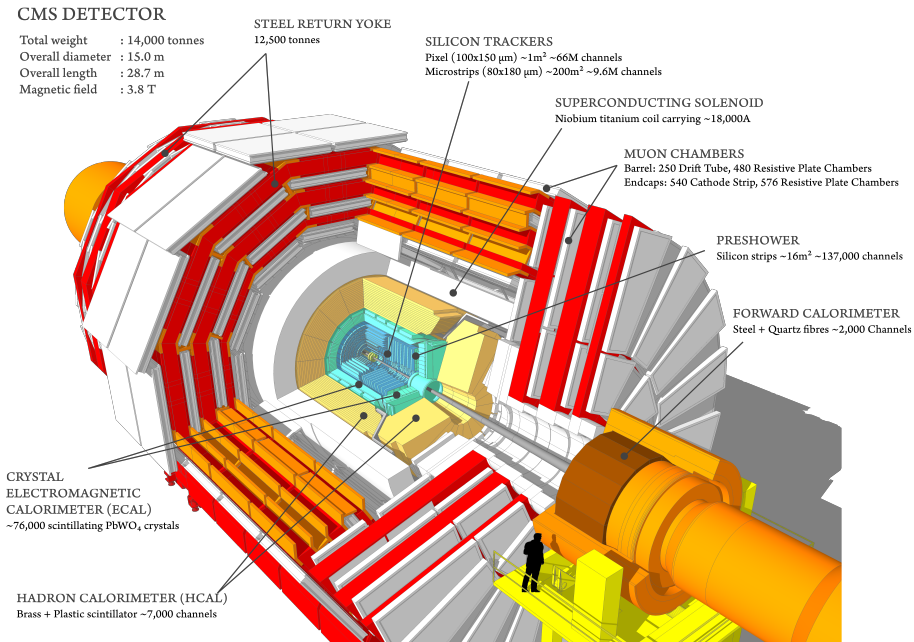


Figure 1.3: CMS Detector Diagram (from [12])

## 1.2.1 Silicon Sensors

The by-product of the collisions hit the silicon sensors before any of the other detector elements, the reason why they are the first items the particles encounter is because they are used to reconstruct the paths of the particle off-spring with extremely high precision - effectively working as electronic ionization chambers. These paths are then used to determine information about what exactly were the by-products of the collisions. Three designs of silicon sensors are used in the CMS Phase-2 Outer Tracker, all of the types used are n-in-p (highly n-doped strips in p-doped bulk) with p-stop strip isolation [1].

### 1.2.1.1 Pixel Detectors

The pixel detector contains about 65 million pixels, allowing it to track the paths of particles emerging from the collision with extreme accuracy due to the sensor being able to activate on a very small area as compared to the strip sensor. It is also the closest detector to the beam pipe, with cylindrical layers at 4cm, 7cm and 11cm and disks at either end [13]. Each of the silicon pixel sensors are  $100\mu m$  by  $150\mu m$ , and each of these pixels are connected via bump-wire-bonds to the channels of the readout electronics. The bump-bonds are tiny solder balls have to be put on every cell with relatively high precision [10].

### 1.2.1.2 Strip Sensors

Directly outside of the region where the silicon pixel detectors are found are the outer tracker modules where two main types are found, the  $2S$  and  $PS$  modules. The  $2S$  modules use two strip sensors with an area of  $10^2 cm^2$ . Now, the  $2S$  sensors are designed with a segmentation along its strips and this results in two rows with 1016 strips with a length of  $5cm$  and a pitch of  $90\mu m$  [10]. Now, the  $PS$  sensors uses a strip ( $PS - s$ ) and a macro-pixel sensor ( $PS - p$ ) with an area of  $5 \cdot 10 cm^2$  each.

# Chapter 2

## Silicon Detectors

The are a number of factors that went into the selection of silicon for the material comprising the particle sensors. Understanding the properties of semiconductor sensors and silicon in general is crucial for the later work that follows, this chapter will sever to briefly summarize some of the main features.

### 2.1 Silicon Sensor Properties

Silicon has four valence electrons, and when it's in crystalline form all four valence electrons are shared in covalent bonds with neighbouring silicon atoms. In order to make the transportation of electrons easier within the lattice of the silicon it is common practice to change the electrical properties of a semiconductor by adding (doping) different elements into the structure of the silicon crystal lattice. There are two types of dopants, the first type adds one additional electron to the lattice region due to their being five valence electrons on the dopant atom. This type of silicon is labeled n-doped and the concentration of donors is typically  $N_D$ , typically phosphorous is used as the donor atom.

The second type adds a positive "hole", the hole is created when the dopant has

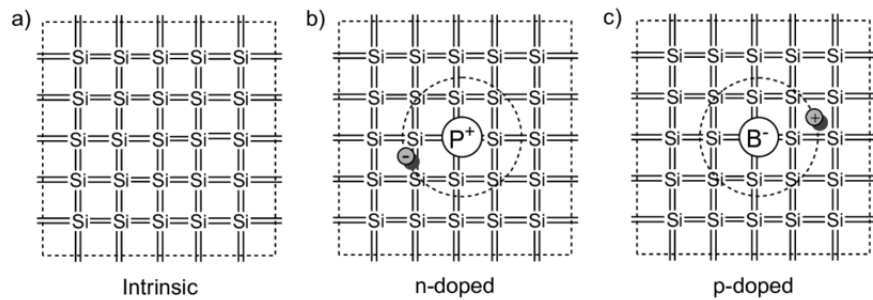


Figure 2.1: Example of doping in Silicon (from [10])

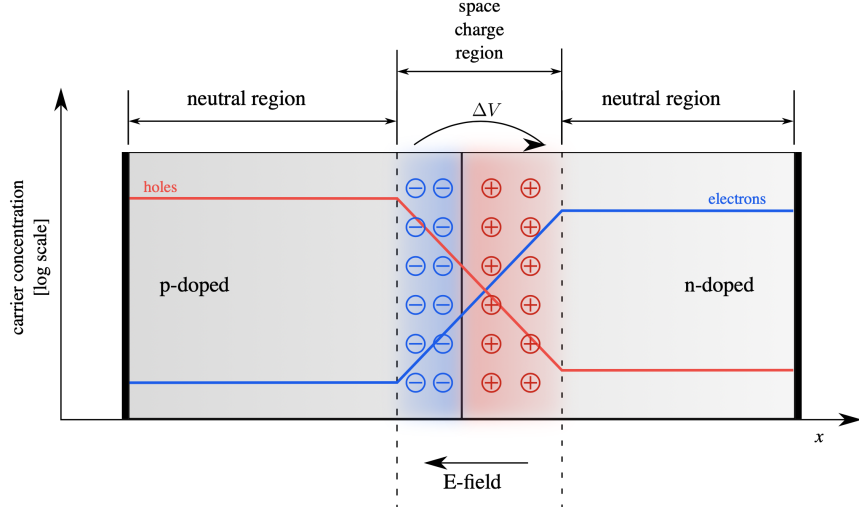


Figure 2.2: Pn-junction under electrically neutral conditions (from [2])

only three valence electrons, and so the region surrounding the dopant is effectively missing one electron. This type of silicon is called p-doped and typically boron or aluminum is used. The concentration of acceptors is labelled  $N_A$ .

In figure 2.1 we can see a pictorial representation of the different silicon types (a) shows Intrinsic silicon, (b) shows a n-type Si with donor (phosphorus). Finally in (c) we see a p-type Si with acceptor (boron). Typical values for the doping concentration range between  $10^{12} \text{ cm}^{-3}$  and  $10^{18} \text{ cm}^{-3}$  [7].

### 2.1.1 PN Junction

In figure 2.2 we see the simplest pn-device which is referred to as a pn-junction. The p-doped and n-doped layers of a diode are sandwiched by two parallel metal electrodes. The configuration is comparable to a plate capacitor. Thus, the capacitance of a diode is given by the field constants  $\epsilon$ , the area of the diode  $A$  and the width of the depletion zone  $w$  seen in equation 2.1:

$$C = \epsilon_0 \epsilon_{Si} \frac{A}{w} \quad (2.1)$$

A positive terminal connected to the p-doped region and a negative terminal connected to the n-doped region will affect the space charge region of the pn-junction by reducing the electric field and thus reducing the width of the depletion region.

This is known as forward biasing, while connecting the terminals the other way around is simply called reverse biasing.

Applying a bias voltage  $V$  in the reverse direction to the sensor, the region of ionized acceptors and donors is named the space-charge-region (which can be seen in figure 2.2) and the effective potential is

$$V + V_{bi} = \frac{1}{e} (E_i^p + E_i^n) = \frac{k_B T}{e} \ln \left( \frac{N_A N_D}{n_i^2} \right) \quad (2.2)$$

Now, the thickness of the space charge region is  $W = d_p + d_n$  and can be given as (calculation found in [6])

$$w(V) = \sqrt{\frac{2\epsilon_0\epsilon_{Si}}{e} \left( \frac{1}{N_A} + \frac{1}{N_D} \right) (V + V_{bi})} \quad (2.3)$$

where  $V_{bi}$  is the so-called built-in-voltage,  $N_A$  is the concentration of acceptor atoms,  $N_D$  is likewise the concentration of donor atoms,  $\epsilon_0$  is the permittivity of vacuum and  $\epsilon_{Si}$  is the permittivity of silicon where  $\epsilon_{Si}/\epsilon_0 \approx 11.8$ . Typically  $V_{bi}$  is usually insignificant compared to the bias applied to the sensors so we can approximate the depletion region as

$$w(V) \approx \sqrt{\frac{2V\epsilon_0\epsilon_{Si}}{eN_D}} \quad (2.4)$$

Now, in order to utilize the entire piece of silicon for detecting particles we need to expand this depletion region over throughout the entire thickness of the silicon detector. The voltage at which this is achieved is called the depletion voltage ( $V_{dep}$ ) and is given by

$$V_{dep} = \frac{eN_D d^2}{2\epsilon_0\epsilon_{Si}} \quad (2.5)$$

In a reverse bias situation the leakage current versus applied voltage follows a characteristic pattern (as seen in figure 2.3). The breakdown is defined as the rapid increase of the current when the reverse bias goes above a certain limit ( $V_{BD}$ ).

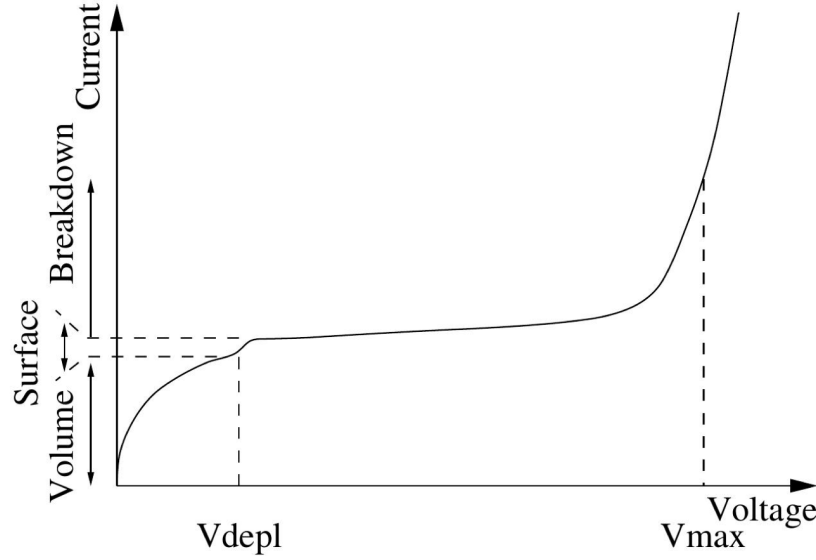


Figure 2.3: Typical IV Curve (from [11])

Now in the case of measuring the capacitance we can refer to the following equation

$$w(V) = \sqrt{\frac{2\epsilon_0\epsilon_{Si}}{e} \left( \frac{1}{N_A} + \frac{1}{N_D} \right) (V + V_{bi})} \quad (2.6)$$

where the built-in voltage  $V_{bi}$  can be neglected because  $V \gg V_{bi}$  is assumed, which is the case in the operation of silicon detectors. The important thing to note is that the depleted region increases linearly with the square root of the bias

Now one could then use eqn. 2.6 and substitute it into eqn. 2.1 to arrive at the following conclusion

$$C = \epsilon_0\epsilon_{Si}A \frac{eN_A N_D}{\sqrt{2\epsilon_0\epsilon_{Si} (N_A + N_D) (V + V_{bi})}} \quad (2.7)$$

We can see that the capacitance will decrease proportionally with the square root of the bias voltage until the region of depletion extends over the entire volume of the diode, we call this phenomena full depletion and label the voltage at which this occurs  $V_{dep}$ . At voltages higher than the depletion voltage we see a constant capacitance where the value of the capacitance for this regime corresponds to the

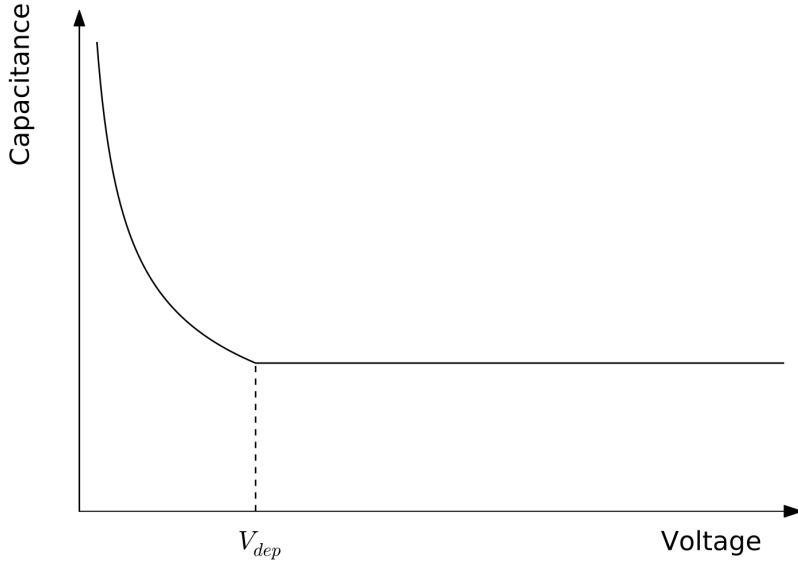


Figure 2.4: Typical CV Curve (from [11])

geometrical capacitance of the diode when considered as a parallel plate capacitor. The value of the capacitance for that situation is:

$$C = \epsilon_0 \epsilon_{Si} \frac{A}{d} \quad (2.8)$$

where  $d$  is simply the total thickness of the diode. Additionally, one can express the reverse current dependence on the temperature by

$$I \propto T^2 \cdot e^{-\frac{E_g}{2k_B T}} \quad (2.9)$$

where  $E_g$  is the energy gap of the silicon being biased. In our own research we found it very useful to be able to convert between leakage currents at one temperature and leakage currents at another temperature, we did that using the following formula

$$I(T) = I_{tot} \cdot \left( \frac{T}{T_0} \right)^2 \cdot e^{-\frac{E_g}{2k_B} \left( \frac{1}{T_0} - \frac{1}{T} \right)} \quad (2.10)$$

where  $I_{tot}$  is the measured leakage current at  $T_0$ ,  $T$  is the temperature,  $E_g$  is the band gap energy of silicon and  $k_B$  is of course the Boltzmann constant. Now, as

we will cover in the following chapter, as silicon is damaged by radiation the leakage current per unit volume  $\Delta I$  increases linearly with fluence  $\Phi_{eq}$  [9], the slope of this linear relationship is called the current related damage constant ( $\alpha$ ) and can be seen in the following equation

$$\Delta I = \alpha \Phi_{eq} V \quad (2.11)$$

# Chapter 3

## Radiation Damage

Generally speaking, in high energy physics (HEP) experiments, the aim of the silicon tracking detectors is the detection of particles passing through the device which makes use of the radiation-matter interactions. Although as one can imagine, the very nature of these interactions can significantly alter the nature of the detector when these kinds of interactions are numerous and over a long period of time. Of course this is of large concern for the HL-LHC upgrade, and so fully characterizing the effects is of great importance. Permanent radiation damage can manifest in two predominate ways, those ways being bulk and surface damage. Though it is the bulk damage which is typically the limiting factor for the use of silicon detectors in HEP experiments, so it is this regime the chapter will primarily focus on. Further reading on bulk damage can be found in the PhD Thesis by Michael Moll [9].

The following chapter will cover radiation damage mechanisms, characterizations of those changes, and the behavior of those changes with respect to temperature after irradiation.

### 3.1 Bulk Silicon Damage

Silicon bulk damage is due primarily to impinging particles hitting silicon atoms out of their original place in the crystal lattice. When an incoming particle first hits a silicon atom in the crystal lattice it is called a "primary knock-on atom" (PKA). The PKA then leaves its original lattice site which results in a silicon interstitial and a vacancy where the atom originally was (Frenkel Pair). What Van Lint found was that the primary recoil atom could only be displaced if the energy imparted by the oncoming particle was more than some displacement threshold energy  $E_d \approx 25\text{eV}$  [16]. One could make a simple non-relativistic calculation for the energy that could

be transmitted via elastic scattering; if the mass of the incident particle is  $m_{incident}$  with kinetic energy  $E_{incident}$  then the maximum energy that could be imparted into the silicon atom in the lattice is

$$E_R = 4 \cdot E_{incident} \cdot \frac{m_{incident} \cdot m_{Si}}{(m_{incident} + m_{Si})^2} \quad (3.1)$$

From the above equation and the displacement threshold energy one could calculate the necessary kinetic energy of the incident particle necessary to displace a silicon atom from the lattice, though this is not something I will do here. Refer to [16] and [9] for more information on the subject.

## 3.2 Non-Ionizing-Energy-Loss (NEIL) Hypothesis

When considering the particles incident on the silicon detectors, its not the charged hadrons we need to worry about too much - this is because they interact primarily by the coulomb interaction and so most of these interactions only lead to ionization. What needs to be considered however are the neutrally charged neutrons which only interact with the nucleus of the silicon atoms. Most of the interactions between neutrons and the silicon nuclei can be modeled as elastic collisions, though at energies above 1.8MeV nuclear reactions can also take place [16].

Now that we know who our likely bulk damaging culprits are (high energy neutrons), we need a way to model how radiation damage scales with particle energy. The model which we use is called the Non-Ionizing-Energy-Loss-Hypothesis, or NEIL hypothesis. The simplifying assumption of the NEIL hypothesis is that the change in the material due to displacement damage scales linearly with the energy of the incident particles, this doesn't account for any spatial considerations of the incident particles or damage due to PKA cascades. In order to arrive at a calculation for the NEIL, one can use the Lindhard-Partition-Function  $P(E_R)$  [6] and then the NEIL can be expressed by the displacement-damage-cross-section

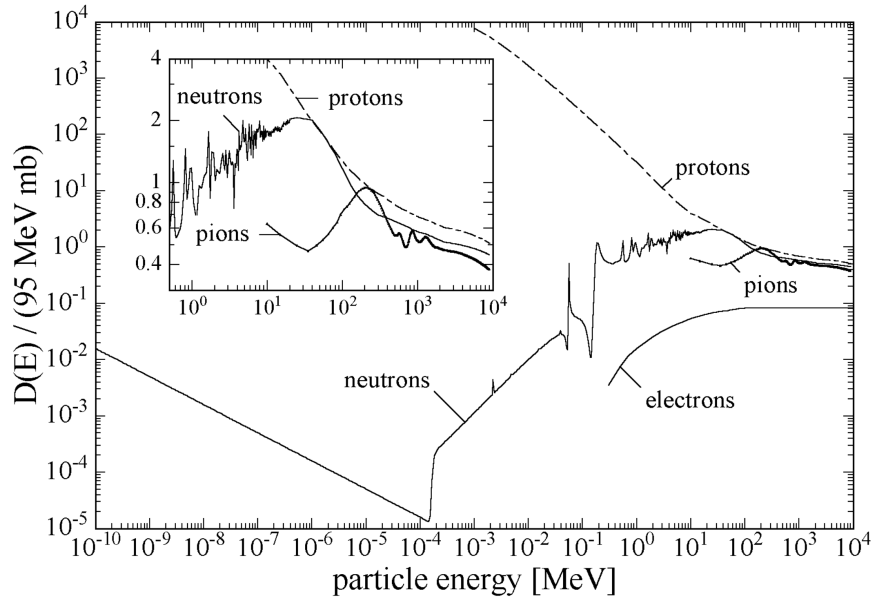


Figure 3.1: Displacement Damage Functions  $D(E)$  (from [9])

$$D(E) := \sum_{\nu} \sigma_{\nu}(E) \cdot \int_0^{E_R} f_{\nu}(E, E_R) P(E_R) dE_R \quad (3.2)$$

where  $\nu$  indicates all possible interactions between the incident particle of energy  $E$  and the silicon atoms in the crystal leading to displacement in the lattice.  $\sigma_{\nu}$  is the cross section corresponding to the reaction,  $f_{\nu}(E, E_R)$  is the probability density function for the generation of a PKA with recoil energy  $E_R$  by a particle with energy  $E$ . This is then integrated over all recoil energies, where a recoil energy less than the threshold displacement energy ( $P(E_R < E_d) = 0$ ) are identically zero [9].

### 3.3 Annealing

#### 3.3.1 Leakage Current

$$\Delta I = \alpha \Phi_{eq} V \quad (3.3)$$

$$\Phi_{eq} = \frac{\Delta I}{\alpha V} \quad (3.4)$$

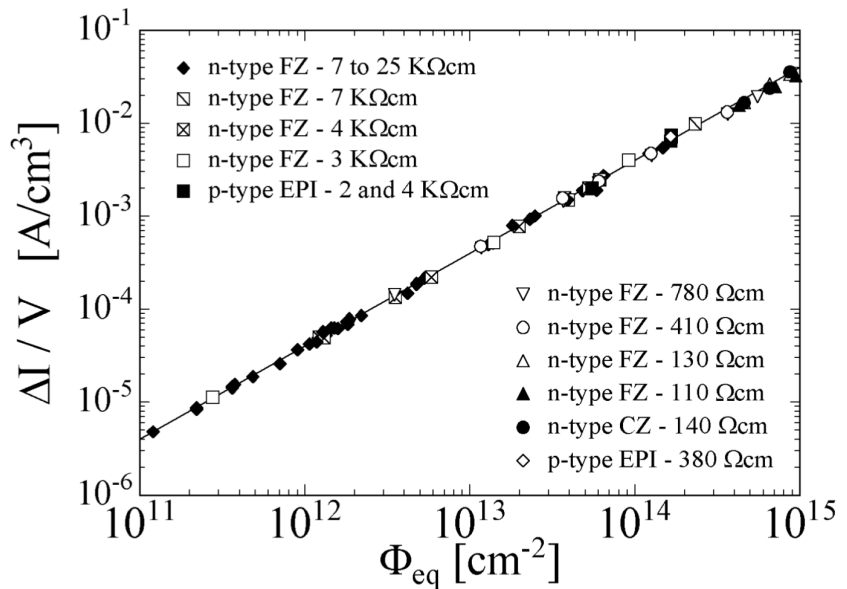


Figure 3.2: Fluence Dependence of Leakage Current for Silicon Detectors (from [9])

Where in our fluence analysis we are using a value of  $\alpha = (3.99 \pm 0.03) \cdot 10^{-17} A/cm$  which we used from the work of R. Wunstorf [18] which was later confirmed by M. Moll [8] to work well for annealing values of 80 min at 60C.

### 3.3.2 Effective Doping Concentration $N_{eff}$

the time dependence of  $N_{eff}$  can be parametrized as

$$\Delta N_{eff}(t) = N_C + N_A(t) + N_Y(t) \quad (3.5)$$

### 3.3.3 Hamburg Annealing Model

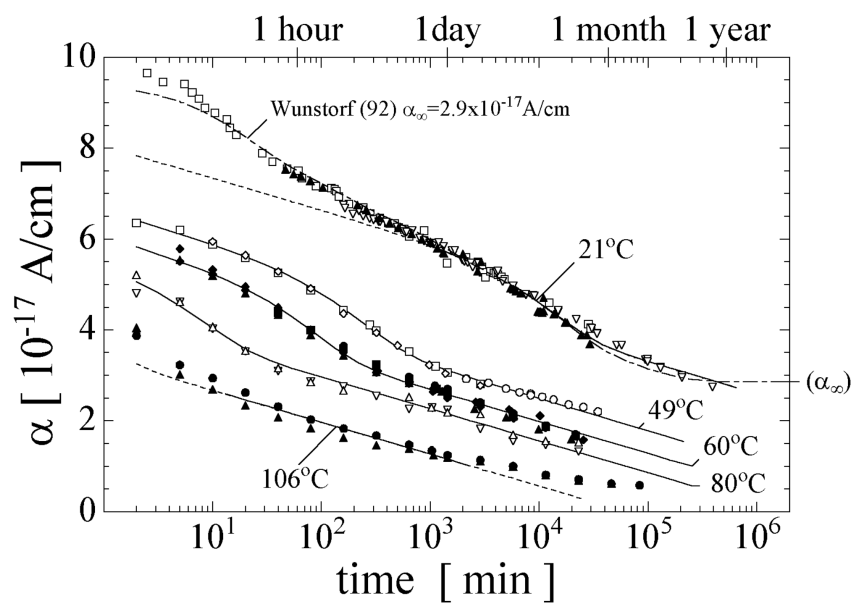


Figure 3.3: Current Related Damage Rate  $\alpha$  as a Result of Cumulated Annealing Times at Different Temperatures (from [9])

# **Chapter 4**

## **Probe Station Experimental Setup**

### **4.1 Test Diodes**

#### **4.1.1 DZero Diodes**

#### **4.1.2 PIN Diodes**

#### **4.1.3 2S and PSS Halfmoon Diodes**

#### **4.1.4 HGCAL Diodes**

### **4.2 Electrical Characterization**

#### **4.2.1 Current-Voltage Measurement (IV)**

#### **4.2.2 Capacitance-Voltage Measurement (CV)**

### **4.3 Environmental Control**

#### **4.3.1 Temperature Control**

#### **4.3.2 Dew-Point Control**

#### **4.3.3 Humidity Control**

# **Chapter 5**

## **Alibava Station Experimental Setup**

### **5.1 Test Diodes**

#### **5.1.1 2S and PSS Halfmoon Diodes**

### **5.2 Radioactive Source**

### **5.3 Environmental Control**

#### **5.3.1 Temperature Control**

#### **5.3.2 Dew-Point Control**

#### **5.3.3 Humidity Control**

### **5.4 Measuring Halfmoon Diodes**

#### **5.4.1 Printed Circuit Board**

# **Chapter 6**

## **Irradiating at RINSC**

### **6.1 Rabbit**

#### **6.1.1 Configuration**

#### **6.1.2 Directionality Studies**

#### **6.1.3 Linear Fluence Intensity Studies**

### **6.2 Beam-Port**

# Chapter 7

## Analysis

### 7.1 Calculating Fluence

#### 7.1.1 PIN Diodes

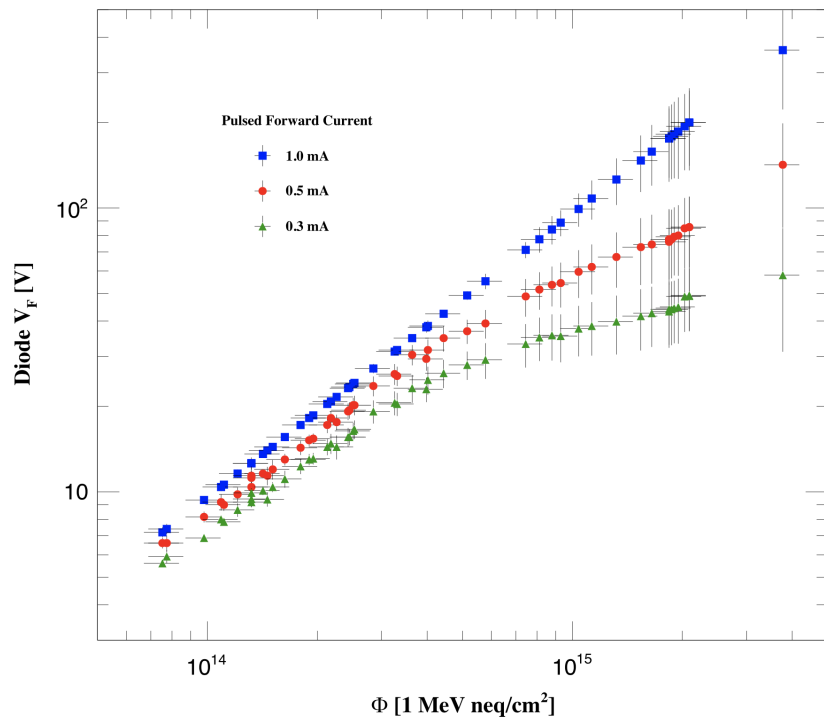


Figure 7.1: PIN Fluence Studies at Different Pulsed Currents (from [5])

In Figure 7.1 from the paper by Hoeferkamp et al. [5], we see diode forward voltage as a function of applied fluence, for three choices of applied current amplitude. The vertical error bars indicate the combined uncertainties related to temperature variation during the irradiation process, current pulse width, and sourcemeter precision. The horizontal error bars indicate the uncertainty deriving from counting statistics on calibration foils in the gamma spectrometer.

Based on the linear fit of Figure 7.1, Hoeferkamp et al. showed a good relation between diode forward voltage and fluence, where the forward voltage was measured after applying a  $1mA$  for approximately .38s. That relation is seen in Equation 7.1.

$$\Phi_{neq} = 1.1 \cdot 10^{13} \cdot V_f - 6.2 \cdot 10^{10} \quad (7.1)$$

### 7.1.2 Depletion Voltage Calculation

### 7.1.3 Current Temperature Conversion

## 7.2 Hamburg Model Analysis

### 7.2.1 Ljubljana Diodes

### 7.2.2 HGCAL Diodes

## 7.3 PIN Analysis

### 7.3.1 Temperature Study

### 7.3.2 Annealing Study

# **Chapter 8**

## **Conclusions**

### **8.1 Use of Diodes in a High Fluence Environment**

#### **8.1.1 PINs**

#### **8.1.2 DZero**

#### **8.1.3 HGCAL**

### **8.2 Affects of Concurrent Annealing and Irradiation**

### **8.3 RINSC Ljubjana Cross Calibration**

#### **8.3.1 Silicon Damage Constant**

# Bibliography

- [1] W. Adam et al. ‘P-Type Silicon Strip Sensors for the new CMS Tracker at HL-LHC’. In: *Journal of Instrumentation* 12.06 (June 2017), P06018–P06018. doi: [10.1088/1748-0221/12/06/p06018](https://doi.org/10.1088/1748-0221/12/06/p06018). URL: <https://doi.org/10.1088/1748-0221/12/06/p06018>.
- [2] Adundovi. *A P-N Junction in Thermal Equilibrium*. URL: [https://en.wikipedia.org/wiki/P-N\\_junction](https://en.wikipedia.org/wiki/P-N_junction).
- [3] Alexander Furgeri. ‘Quality assurance and irradiation studies on CMS silicon strip sensors’. PhD thesis. Karlsruhe U., 2006.
- [4] Julie Haffner. ‘The CERN accelerator complex. Complexe des accélérateurs du CERN’. In: (Oct. 2013). General Photo. URL: <https://cds.cern.ch/record/1621894>.
- [5] M.R. Hoeferkamp et al. ‘Application of p-i-n photodiodes to charged particle fluence measurements beyond  $10^{15}$  1-MeV-neutron-equivalent/cm<sup>2</sup>’. In: *Nuclear Instruments and Methods in Physics Research Section A: Accelerators, Spectrometers, Detectors and Associated Equipment* 890 (2018), pp. 108–111. ISSN: 0168-9002. doi: <https://doi.org/10.1016/j.nima.2018.02.070>. URL: <https://www.sciencedirect.com/science/article/pii/S0168900218302249>.
- [6] Gerhard Lutz. *Semiconductor Radiation Detectors*. Berlin: Springer, 1999. URL: <https://cds.cern.ch/record/887388>.
- [7] Marius Metzler. ‘Irradiation studies on n-in-p silicon strip sensors in the course of the CMS Phase-2 Outer Tracker Upgrade’. PhD thesis. Karlsruhe Institute of Technology (KIT), 2020.
- [8] Michael Moll. ‘Displacement Damage in Silicon Detectors for High Energy Physics’. In: *IEEE Transactions on Nuclear Science* 65.8 (2018), pp. 1561–1582. doi: [10.1109/TNS.2018.2819506](https://doi.org/10.1109/TNS.2018.2819506).

- [9] Michael Moll. ‘Radiation damage in silicon particle detectors: Microscopic defects and macroscopic properties’. PhD thesis. Hamburg U., 1999.
- [10] Jason Röhr. ‘Electron Transport in Solution Processed Antimony Sulphide Thin Films made from a Xanthate Precursor’. PhD thesis. Sept. 2014. DOI: [10.13140/RG.2.2.29530.39366](https://doi.org/10.13140/RG.2.2.29530.39366).
- [11] Leonardo Rossi et al. *Pixel detectors: from fundamentals to applications*. Particle acceleration and detection. Berlin: Springer, 2006. DOI: [10.1007/3-540-28333-1](https://doi.org/10.1007/3-540-28333-1). URL: <https://cds.cern.ch/record/976471>.
- [12] Tai Sakuma. ‘Cutaway diagrams of CMS detector’. In: (May 2019). URL: <https://cds.cern.ch/record/2665537>.
- [13] *Silicon Pixels Sensors at CMS*. URL: <https://home.cern/science/accelerators/large-hadron-collider>.
- [14] *The High-Luminosity large Hadron Collider*. URL: <https://home.cern/resources/faqs/high-luminosity-lhc>.
- [15] *The Large Hadron Collider*. URL: <https://home.cern/science/accelerators/large-hadron-collider>.
- [16] V A.J Van Lint et al. ‘Mechanisms of radiation effects in electronic materials. Vol. 1’. In: (Jan. 1980). URL: <https://www.osti.gov/biblio/6854931>.
- [17] Pascal Vanlaer et al. ‘The Phase-2 Upgrade of the CMS Tracker’. In: 2017.
- [18] Renate Wunstorf. ‘Systematische Untersuchungen zur Strahlenresistenz von Silizium-Detektoren für die Verwendung in Hochenergiephysik-Experimenten’. University of Hamburg, Diss., 1992. Dr. Hamburg: University of Hamburg, 1992. URL: <https://bib-pubdb1.desy.de/record/153817>.

# Appendix A

## Code and Data Location

1. GitHub CMS Folder:

[https://github.com/AndrewTKent/CERN\\_CMS\\_Silicon\\_Sensor](https://github.com/AndrewTKent/CERN_CMS_Silicon_Sensor)

2. Annealing Temperature Conversion:

[https://github.com/AndrewTKent/CERN\\_CMS\\_Silicon\\_Sensor/tree/main/Diodes/DZero/Annealing\\_Conversion](https://github.com/AndrewTKent/CERN_CMS_Silicon_Sensor/tree/main/Diodes/DZero/Annealing_Conversion)

3. HGCAL Hamburg Analysis:

[https://github.com/AndrewTKent/CERN\\_CMS\\_Silicon\\_Sensor/tree/main/Diodes/HGCAL/Hamburg\\_Analysis](https://github.com/AndrewTKent/CERN_CMS_Silicon_Sensor/tree/main/Diodes/HGCAL/Hamburg_Analysis)

4. Alibava Annealing Studies:

[https://github.com/AndrewTKent/CERN\\_CMS\\_Silicon\\_Sensor/tree/main/Diodes/Halfmoon/Annealing](https://github.com/AndrewTKent/CERN_CMS_Silicon_Sensor/tree/main/Diodes/Halfmoon/Annealing)

5. Ljubljana vs. Rinsc Analysis:

[https://github.com/AndrewTKent/CERN\\_CMS\\_Silicon\\_Sensor/tree/main/Diodes/Ljubljana\\_Diodes](https://github.com/AndrewTKent/CERN_CMS_Silicon_Sensor/tree/main/Diodes/Ljubljana_Diodes)

6. Pin Diodes:

[https://github.com/AndrewTKent/CERN\\_CMS\\_Silicon\\_Sensor/tree/main/Diodes/Pins](https://github.com/AndrewTKent/CERN_CMS_Silicon_Sensor/tree/main/Diodes/Pins)